JACS
JOURNAL OF THE AMERICAN CHEMICAL SOCIETY

UNIVERSITY OF BIRMINGHAM

Subscriber access provided by University of Birmingham

Article

Excited State Turn-On of Aurophilicity and Tunability of Relativistic Effects in a Series of Digold Triazolates Synthesized via iClick

Charles J. Zeman, Yu-Hsuan Shen, Jessica Heller, Khalil A. Abboud, Kirk S. Schanze, and Adam S. Veige

J. Am. Chem. Soc., **Just Accepted Manuscript** • DOI: 10.1021/jacs.0c01624 • Publication Date (Web): 08 Apr 2020

Downloaded from pubs.acs.org on April 13, 2020

Just Accepted

"Just Accepted" manuscripts have been peer-reviewed and accepted for publication. They are posted online prior to technical editing, formatting for publication and author proofing. The American Chemical Society provides "Just Accepted" as a service to the research community to expedite the dissemination of scientific material as soon as possible after acceptance. "Just Accepted" manuscripts appear in full in PDF format accompanied by an HTML abstract. "Just Accepted" manuscripts have been fully peer reviewed, but should not be considered the official version of record. They are citable by the Digital Object Identifier (DOI®). "Just Accepted" is an optional service offered to authors. Therefore, the "Just Accepted" Web site may not include all articles that will be published in the journal. After a manuscript is technically edited and formatted, it will be removed from the "Just Accepted" Web site and published as an ASAP article. Note that technical editing may introduce minor changes to the manuscript text and/or graphics which could affect content, and all legal disclaimers and ethical guidelines that apply to the journal pertain. ACS cannot be held responsible for errors or consequences arising from the use of information contained in these "Just Accepted" manuscripts.

is published by the American Chemical Society. 1155 Sixteenth Street N.W., Washington, DC 20036
Published by American Chemical Society. Copyright © American Chemical Society. However, no copyright claim is made to original U.S. Government works, or works produced by employees of any Commonwealth realm Crown government in the course of their duties.

Excited State Turn-On of Aurophilicity and Tunability of Relativistic Effects in a Series of Digold Triazolates Synthesized via iClick

Charles J. Zeman IV,[a,b] Yu-Hsuan Shen,[a] Jessica K. Heller,[a] Khalil A. Abboud,[a] Kirk S. Schanze,[*b] Adam S. Veige,[*a]

[a]University of Florida, Department of Chemistry, Center for Catalysis, P.O. Box 117200, Gainesville, FL, 32611.

[b]University of Texas at San Antonio, Department of Chemistry, One UTSA Circle, San Antonio, TX 78249.

ABSTRACT: iClick reactions between Au(I) acetylides PPh_3Au-C≡CR where R = nitrophenyl ($PhNO_2$), phenyl (Ph), thiophene (Th), bithiophene (biTh), and dimethyl aniline ($PhNMe_2$) with Au(I)-azide PPh_3AuN_3 provide digold complexes of the general formula R-1,5-*bis*-triphenylphosphinegold(I) 1,2,3-triazolate (**Au_2-R**). Within the digold triazolate complexes the Au(I) atoms are held in close proximity but beyond the distance typically observed for aurophilic bonding. Though no bond exists in the ground state, time-dependent density functional theory interrogation of the complexes reveals excited states with significant aurophilic bonding. The series of complexes allows for tuning of the excited state "turn-on" of aurophilicity, where ligand to metal charge transfer (LMCT) induces the aurophilic bonding. Complexes containing ligand localized excited states however, do not exhibit aurophilicity in the excited state. As a control experiment, a monogold complex was synthesized. The computed excited state of the monogold species exhibited LMCT to the gold ion as in the dinuclear cases, but without a partnering gold ion only a distinct N-Au-P bending occurs revealing a potential mechanism for the excited state turn-on of aurophilic bonding. Analysis of the steady-state electronic spectra indicate that LMCT states are achievable for compounds with sufficiently strong electron donating ligands, and in digold complexes this is associated with enhanced fluorescence, suggestive of an aurophilic interaction.

INTRODUCTION

Aurophilicity is the term given for the peculiarly strong bond (7 – 12 kcal/mol binding energy) between the metal centers of Au(I) complexes.[1–3] Smaller than the sum of the two van der Waals radii (3.8 Å), inter- and intramolecular aurophilic bonds exhibit Au(I)-Au(I) equilibrium distances between 2.5 – 3.5 Å.[3] The observed bond length depends greatly on steric limitations, with large ligands obstructing close contacts such that formal definitions of aurophilicity set the cutoff distance as 3.5 Å, but any distance between 3.5 and 3.8 Å is considered to be ambiguous.[2–6]

Comprised of two closed shell atoms with $5d^{10}$ electron configurations, the peculiar aspect of the aurophilic bond is that the atoms are not expected to experience attractive forces through ordinary effects. Intuitively, the +1 formal charge of gold cations is expected to give rise to significant Coulombic repulsion within short distances from one another. These contrarian physical properties of Au(I) beg the question of why there should be any attractive forces present at all. Evidence for Au(I)-Au(I) bonds began to accumulate in the 1970s, though the term "aurophilicity" was not coined until 1988 when relativistic effects of electrons in gold atoms were implicated.[7–9] More specifically, similar to Van der Waals theory,[10] electron correlation energy is the primary contributor to the attractive force between the two Au(I) metal atoms.[2] Known to be at a local maximum on the periodic table for gold atoms,[5,11–14] it is the relativistic expansion of *d*-orbitals that induces the interaction leading to aurophilicity, referred to as "super van der Waals" or "relativistic bonding."[6] Theoretical treatments approximate 28% of the electron correlation induced binding interaction between Au(I) atoms is due to relativistic augmentation.[10] Supporting this contention, Hartree-Fock methods, which do not include Coulombic correlation contributions to the total energy, fail to model aurophilicity.[15–17]

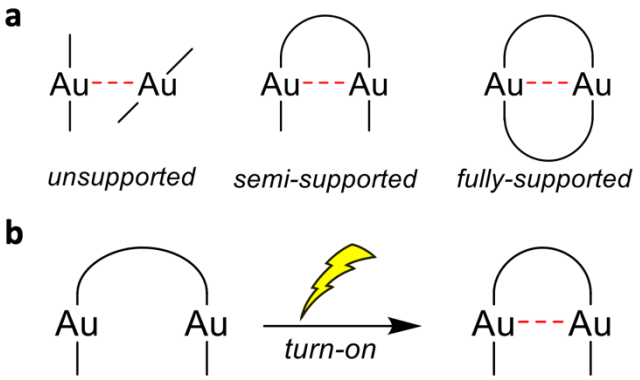

Figure 1. (a) Classes of aurophilic bonding. (b) *This work*, excited state "turn-on" of aurophilic bonding.

Complexes featuring Au(I)-Au(I) bonds come in three forms: 1) intermolecular unsupported, 2) intramolecular semi-supported, and 3) intramolecular fully-supported bonds (Fig. 1a). Often provided as evidence for the existence of aurophilicity, compounds containing Au(I)-Au(I) bonds exhibit intense luminescence in the solid state.[18–21] However, the Au(I)-Au(I) bond often breaks upon dissolving the complexes in solution and only a few unsupported soluble

complexes featuring aurophilic bonds are known.[20,22–25] Materials applications of aurophilicity are rare, and despite decades of work to understand the nature of the interaction, only recently a gold cluster featuring aurophilic bonds was incorporated into an organic light-emitting diode (OLED); furthermore, only three systems[26–29] have been shown to provide white light. More importantly, solution phase processing of opto-electronic materials is obviously advantageous. However, unsupported aurophilic bonds are generally only stable in the solid state. One possible solution is to design complexes that do not have aurophilic bonds in the ground state but rather upon photoexcitation induce the interaction in the excited state (Fig. 1b).

It is well understood that Au(I)-Au(I) bonds that are present in the ground state will contract upon photoexcitation.[30,31] Some examples even exhibit excited state aurophilic interactions where the ground state distance between gold atoms was long, yet still within the accepted range for aurophilic interactions.[32] For example, Tobon, Saillard, Liu, Boucekkine et al. demonstrated both theoretically and experimentally that a fully-supported digold complex can undergo contraction from 3.32 to 2.61 Å in the excited state.[33] Similar studies of photoinduced structural change have even been extended to diPt(II) complexes.[34,35]

Inorganic click or "iClick" involves adapting typically all-organic click reactions to include metal ions. For example, combining Ph_3PAu^I-N_3 (**1**) with Ph_3PAu^I-CCPh (**2**) results in the formation of the digold triazolate complex 4-phenyl-1,5-*bis*-triphenylphosphinegold(I) 1,2,3-triazolate (**Au_2-Ph**; Fig. 2). The synthesis of digold complexes is generic and most any alkyne substituent is tolerable. Synthesized for control experiments to delineate the effects of the proximal Au(I) ions, treating the Au(I)-azide complex **1** with 2-ethynylthiophene provides the monogold complex **4,5-Au_1-Th** in 91.1 % yield.

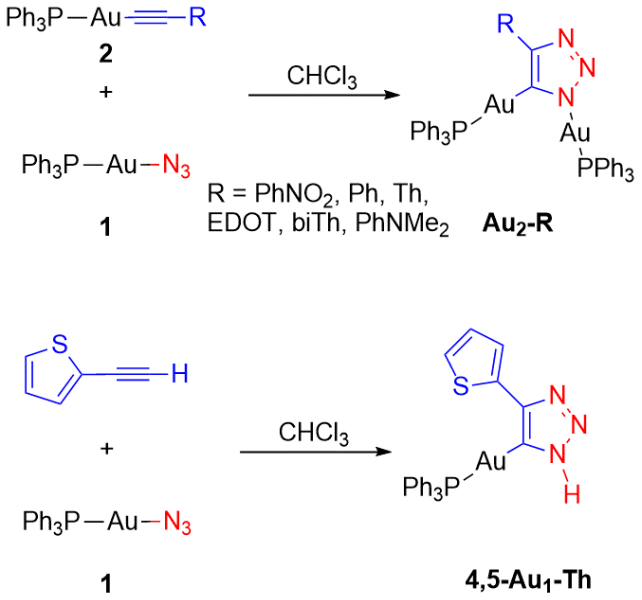

Figure 2. Top: Typical iClick synthesis of digold triazolate **Au_2-Ph**. Bottom: Synthesis of **4,5-Au_1-Th**.

It became immediately apparent by crystallography, computational modeling, and photophysical characterizations that compounds such as **Au_2-Ph** do not have Au(I)-Au(I) bonds in the ground state. At a distance of 3.9 Å, the Au(I)-Au(I) distance is well beyond the accepted cutoff distance for aurophilicity. However, during the course of investigating the photophysical properties and computational analysis of the resulting excited states of the related *flourenyl* derivative **Au_2-FO**,[28] we found evidence for an excited state "turn on" of aurophilic bonding.

As identified through time-dependent density functional theory (TDDFT), a geometry optimization of the excited state S_1 of **Au_2-FO** revealed the interatomic Au(I)-Au(I) distance contracts to 3.5 Å after photoexcitation (Fig. 3). As noted above, this distance is less than the sum of the Van der Waals radii of the two atoms (3.8 Å). By analysis of the charge difference density (CDD) of the excited state S_1, the fluorenyl moiety enables strong ligand to metal charge transfer (LMCT) resulting in an increase in electron density at the Au(I) ions in the excited state. This creates a shorter separation distance of the potential energy minimum of the two-coordinate Au(I) atoms compared to their ground state positions. Presumably, the increase in the effective size of the Van der Waals radii from LMCT enables the Au(I)-Au(I) bonding between the two metal centers where such an interaction would otherwise be unfeasible in the ground state.

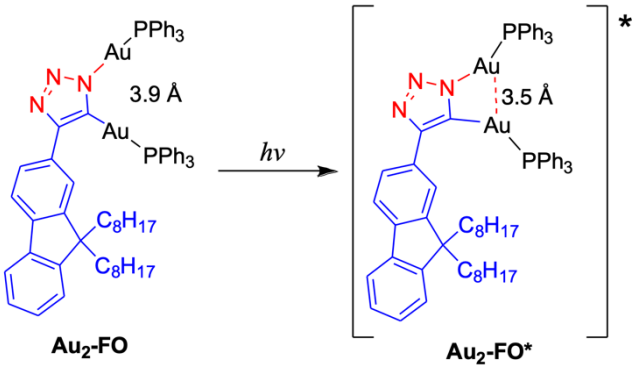

Figure 3. Structure of **Au_2-FO** with illustration of excited state turn-on of an aurophilic interaction where Au atoms separated by 3.9 Å contract to 3.5 Å upon photo excitation.

In this work, we report a series of digold complexes outlined by Figure 4 that contain Au(I) ions well-separated and beyond the limit of aurophilicity in the ground state, but upon photoexcitation, the distance contracts to induce aurophilic bonding in the excited state (Fig. 3) as identified by computational means and further characterized spectroscopically. These compounds were chosen for the range of electron donating strengths presented by the aryl chromophore. Importantly, the observation of excited state "turn on" of a Au(I)-Au(I) interaction is dependent on these electron donating properties of the ligand substituents, thus offering an ability to fine-tune the interaction.

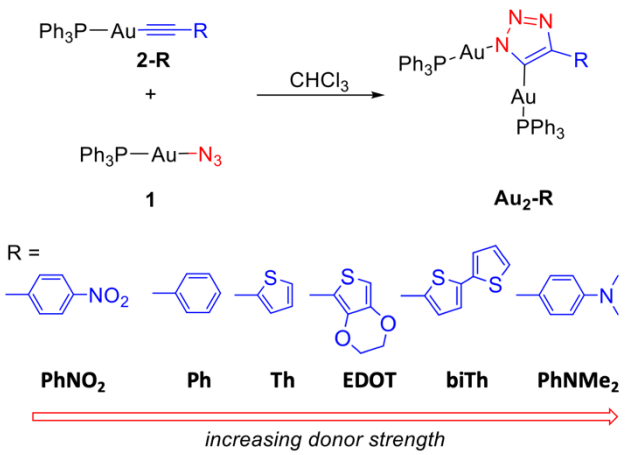

Figure 4. Synthesized compounds by iClick with nitrophenyl ($PhNO_2$), phenyl (Ph), thiophene (Th), bithiophene, (biTh) and dimethyl aniline ($PhNMe_2$) ligands, where the 3,4-ethylenedioxythiophene (EDOT) ligand was only studied computationally.

RESULTS

Preliminary Remarks. Using similar computational methods for diAu(I) complexes of the same model structure in **Au_2-FO**,[28] but exchanging the fluorenyl substituent for any number of moieties with varying degrees of electron donating or withdrawing character will probe the electronic requirements to achieve excited sate turn-on of aurophilic bonding. Figure 4 depicts the structures chosen for this study. Chosen to span a range of relevant ionization potentials (IPs) relative to the electron affinity of Au(I) ions, the substituents should be sufficient at probing the effects of donor strength on excited state turn-on of aurophilicity. Additionally, being analogous to complex **Au_2-FO** allows for the synthesis of this series of similar compounds using the same iClick reaction.[36] Reported previously in the literature are complexes **Au_2-Ph** and **Au_2-$PhNO_2$**, whereas **Au_2-EDOT** was only investigated computationally. Synthetic details and characterization data for new complexes **Au_2-Th**, **Au_2-biTh**, and **Au_2-$PhNMe_2$** are detailed in the supporting information. All compounds were stored under inert atmospheres and isolated from direct exposure to light. Typically, all products exhibited air sensitivity and were handled in an inert atmosphere, the most sensitive being **Au_2-$PhNMe_2$** and the most stable being **Au_2-$PhNO_2$**.

Au_2-Ph, and **Au_2-$PhNO_2$** are crystalline compounds and single crystal X-ray diffraction data is available from the literature.[37,38] For the complexes **Au_2-$PhNMe_2$**, **Au_2-Th** and **Au_2-biTh**, X-ray structural data was acquired to assess the influence, if any, the substituents have on the intramolecular Au(I)-Au(I) bond distance. Figure 5 presents the molecular structures for the model complexes derived from the X-ray structures. Each complex adopts the same general molecular structure in the solid state, where the substituent and the triazolate are rings are nearly coplanar. The Au(I) ions occupy positions 1 and 5 on the triazolate rings. The identity of the substituents does influence the intramolecular Au(I) distances, but all of them are beyond the acceptable cut-off for aurophilic bonding or display inconclusive Au(I)-Au(I) interaction distances at 3.7359(2) 3.7298(2), 3.5642(6), 3.5239(6), 3.4940(3) Å, for **Au_2-$PhNMe_2$**, **Au_2-$PhNO_2$**, **Au_2-biTh**, **Au_2-Th**, and **Au_2-Ph**.

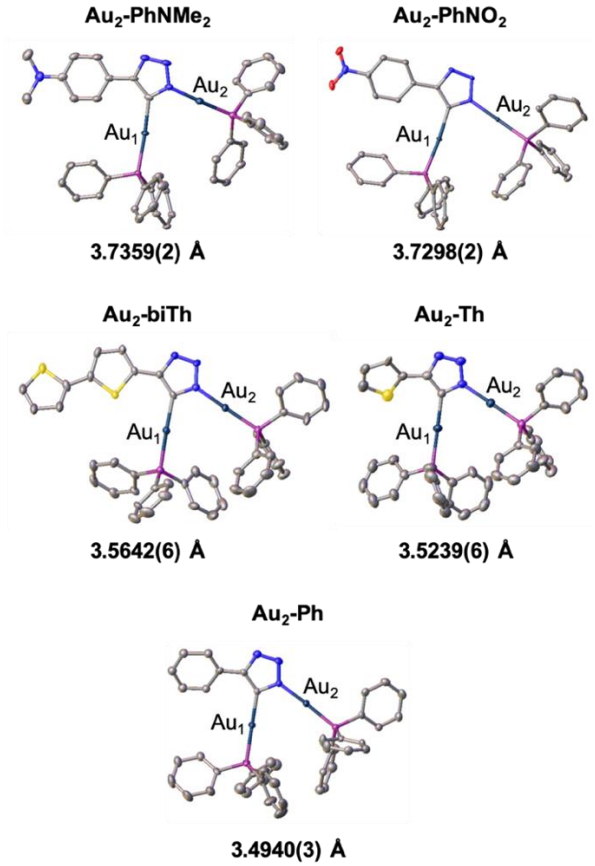

Figure 5. Crystal structures taken from X-ray diffraction results of single crystals.

Computational Modeling. Hartree-Fock (HF), second-order Moeller-Plesset perturbation theory (MP2),[39] Becke's three-parameter hybrid functional (B3LYP),[40–42] and the long-range corrected variant CAM-B3LYP[43] levels of theory were employed to optimize the ground state (S_0) geometries for compounds with triphenyl phosphine ligands replaced with trimethyl phosphine ligands to reduce computational costs (for validation, see supporting information). Of these methods, HF is the only level of theory that does not account for electron correlation energy. In turn, MP2 includes this contribution to the total energy as an adjustment

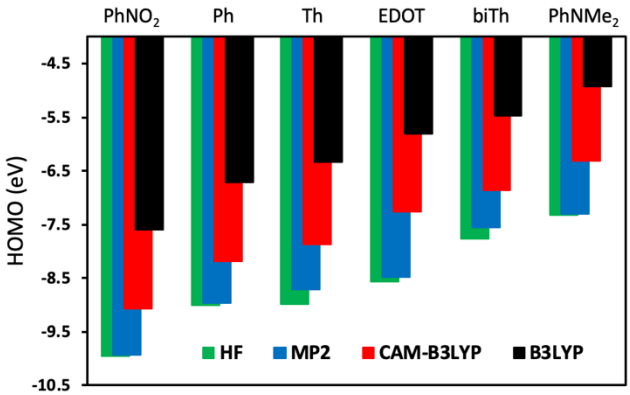

Figure 6. HOMO energy levels (-IP) of the aryl R-groups according to different methods.

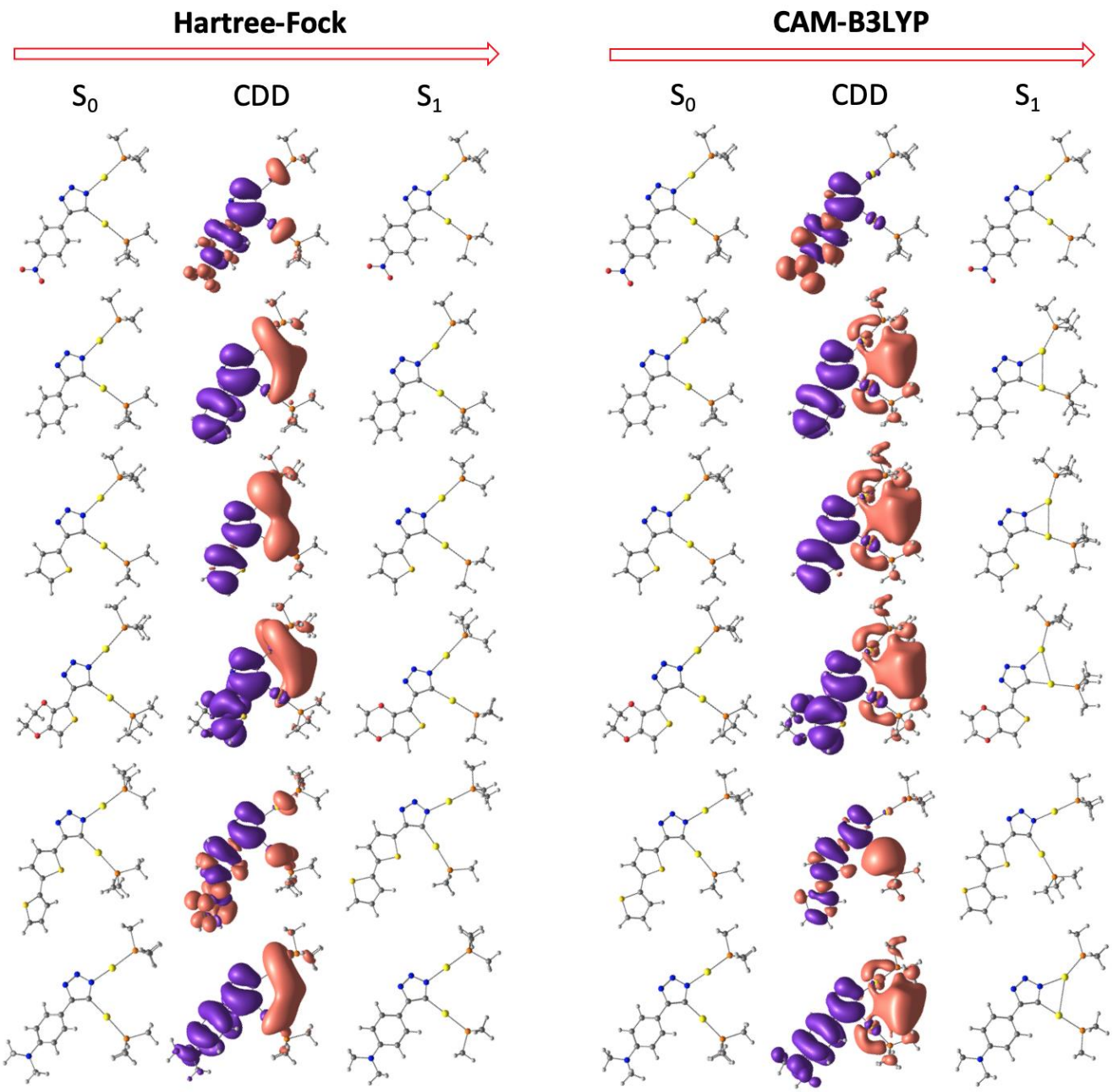

Figure 7. Results of computational modeling of digold triazolates of varying -R groups according to Hartree-Fock (left) and CAM-B3LYP (right). The structures show the optimized ground state geometry (S_0), the charge difference density which moves from purple to pink MOs upon photoexcitation (CDD), and the subsequent relaxed excited state geometry (S_1) sequentially (red arrows). From top to bottom, these structures correspond to **Au_2-$PhNO_2$**, **Au_2-Ph**, **Au_2-Th**, **Au_2-EDOT**, **Au_2-biTh**, and **Au_2-$PhNMe_2$**.

to the Hamiltonian while maintaining the exact solution of the electron exchange energy from pure HF. B3LYP also accounts for both the exchange and correlation potential, through an iterative optimization. Finally, CAM-B3LYP improves on B3LYP by more accurately describing charge separation at greater distances, which is vital for modeling excited states expected to display charge-transfer character. MP2 and CAM-B3LYP are expected to most accurately model the electronic structures for this series of compounds. The results of the ground state geometry optimizations, including the interatomic distance between gold(I) metal centers for each compound are shown in the supporting information (SI). Generally, all methods predict the gold(I) atoms reside at a distance from one another that is larger than the sum of their Van der Waals radii, with MP2 predicting the shortest distance of 3.726 Å for **Au_2-$PhNO_2$**, and HF predicting the longest distance of 3.987 Å for **Au_2-Ph**. From these results alone, no immediately apparent trend is evident across the series of aryl donor moieties.

To better evaluate the relationship between donor character and subsequently determined properties, the IP of each R-group was assumed to be equivalent to the negative of the HOMO energy level, as postulated by Koopman's theorem. Figure 6 depicts these HOMO energies. For the purpose of these calculations, the triazolate was replaced with

a hydrogen atom to isolate the aryl R-group donors. Reported IPs represent those from fully optimized geometries. The results indicate the chosen compounds display a wide range of reducing electron donor strength, with nitrophenyl ($PhNO_2$) being the hardest to oxidize (lowest energy HOMO) and dimethyl aniline ($PhNMe_2$) being the easiest (highest energy HOMO).

For the sake of consistency, excited state analyses employ time dependent (TD) methods throughout. Moreover, no excited state methods exist for MP2,[39] CIS is difficult to make meaningful comparisons with TDDFT by way of employing an alternative method for characterizing excited states,[44] and analytical gradients are unavailable for CIS(D)[45] making geometry optimizations of excited states identified by this method require a prohibitive number of energy calculations. Only a single excitation was calculated with singlet multiplicity, as the lowest lying excited state is the only one of interest and subsequent geometry optimizations ultimately lead to excitation energies that are relaxed to a minimum. As such, optimizations of higher ordered excited states identified by TDDFT become redefined as S_1 upon completion of the calculation. For all compounds, S_1 was comprised of a wide active space with several 1-electron transitions being involved in the configuration interaction (CI). In these CIs, the HOMO-LUMO transition dominates. Figure 7 depicts charge difference densities (CDDs) derived from a coefficient-weighted summation of contributing 1-electron molecular orbital (MO) transitions where charge moves from purple to pink MOs. In all cases, the HOMO (or electron holes in the case of the CDDs) are π MOs that are predominately localized on the aryl-triazolate ligand. In contrast, the LUMO is localized on the metal centers and phosphine ligands for all compounds other than **Au_2-$PhNO_2$** and **Au_2-biTh**. From natural bond orbital (NBO) analysis, it was found that the LUMOs of **Au_2-Ph**, **Au_2-Th**, **Au_2-EDOT**, and **Au_2-$PhNMe_2$** are comprised of approximately 40% gold atomic orbitals of predominately p-character with minimal (< 3%) contribution from phosphorous atoms (Fig. S41). These results indicate S_1 is a LMCT state for aryl R-groups with sufficiently low IPs and high LUMO energy. As such, **Au_2-$PhNO_2$** and **Au_2-biTh** display only a ligand-localized excitation with minimal contributions from the gold(I) atoms. One last noteworthy result is that TDDFT methods predict a greater delocalization of the metal-centered virtual orbitals compared to TDHF.

Table 1. TDDFT Results for Au_2-R Complexes.

Method	-R	ΔE (eV)[a]	f[b]	CT? (Y/N)[c]	ΔR[d] (Å)
TD-HF	**$PhNO_2$**	4.56	0.4812	N	-0.021
	Ph	4.66	0.0441	Y	-0.004
	Th	4.45	0.1493	Y	-0.004
	EDOT	4.84	0.0534	Y	-0.094
	biTh	4.17	0.4956	N	+0.027
	$PhNMe_2$	4.57	0.0399	Y	-0.173
CIS	**$PhNO_2$**	4.70	0.4695	N	-0.028
	Ph	4.69	0.0306	Y	-0.075
	Th	4.54	0.1320	Y	-0.046
	EDOT	4.87	0.0273	Y	-0.051
	biTh	4.32	0.4962	N	+0.023
	$PhNMe_2$	4.60	0.0253	Y	-0.162
TD-B3LYP	**$PhNO_2$**	3.20	0.4983	N	-0.045
	Ph	3.08	0.0001	Y	-0.163
	Th	2.88	0.0001	Y	-0.307
	EDOT	2.87	0.0001	Y	-0.322
	biTh	2.76	0.0000	Y	-0.235
	$PhNMe_2$	2.69	0.0002	Y	-0.312
TD-CAM	**$PhNO_2$**	3.83	0.5437	N	+0.038
	Ph	3.89	0.0016	Y	-0.734
	Th	3.78	0.0001	Y	-0.838
	EDOT	3.81	0.0041	Y	-0.800
	biTh	3.44	0.5276	N	+0.058
	$PhNMe_2$	3.60	0.0006	Y	-0.684

[a]Energy of the vertical excitation, [b]oscillator strength, [c]charge transfer character as identified by CDDs, and [d]the change in the Au(I)-Au(I) distance upon relaxation of the excited state.

Presented in Figure 7 and Table 1 are the ways in which the Au(I)-Au(I) interaction changes in the excited state, while all of the Au(I)-Au(I) distances at the stationary point of the relaxed geometries are given in the SI. Generally, the results indicate excited states identified through TDHF experience minimal structural change upon relaxation. In contrast, a contraction in the Au(I)-Au(I) distance for vertical excitations that display charge-transfer character to the metal centers are observed for TDDFT optimized excited states. These contractions all reach values that are well below the sum of the Van der Waals radii for the two Au(I) atoms. A bending of the angle between N-Au-P atoms from approximately 180° to 120° accompanies the Au(I)-Au(I) contractions in all the examples. Changes in bond angles between Au and the triazolate ring were minimal. These effects were most extreme for CAM-B3LYP, which predicted bond formation between Au atoms within 3.2 Å of one another for **Au_2-Ph**, **Au_2-Th**, **Au_2-EDOT**, and **Au_2-$PhNMe_2$**. Table 1 summarizes the computational results including greater detail regarding the properties of each individual vertical excitation. That is, CT transitions have lower oscil-

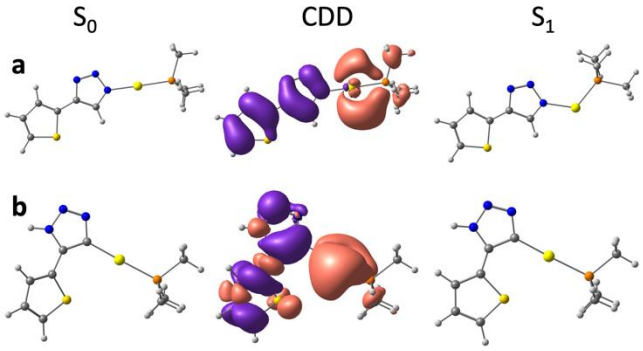

Figure 8. Excited state analysis of (**a**) theoretical **1,4-Au_1-Th** and (**b**) the as synthesized **4,5-Au_1-Th** isomers of the monogold triazolate with a thiophene ligand using CAM-B3LYP.

lator strengths than localized excitations, and excitation energy becomes lower with decreasing IP of the aryl donor. For completeness, calculations at the CAM-B3LYP level of theory were repeated for triplet states, the results of which are shown in Figure S42. It was found that the lowest energy triplet excited states for all compounds were significantly more delocalized compared to singlet excited states, with ligand-centered π-π* character. These findings are consistent with previous work and what is known about triplet excited states in organometallic complexes.[28,36,46,47] Without the distinctive LMCT character of the singlet excited states (Fig. 7), it was not unexpected that no contraction in the Au(I)-Au(I) interatomic distance was observed for any compound when relaxing the excited triplet state geometry.

As a control, and to distinguish the spectroscopic features arising from the excited state turn on of Au(I)-Au(I) bonding, the monogold complex **4,5-Au$_1$-Th** was synthesized (see SI) and subjected to the same (CAM-B3LYP) computational analysis as the digold compounds (Fig. 8). In addition to the synthesized **4,5-Au$_1$-Th** isomer, the **1,4-Au$_1$-Th** isomer was treated computationally. These results show a similar charge-transfer to the Au(I) center, and subsequent optimization of the excited state reveals a significant bending distortion of the N-Au-P bond angle. Naturally, without a second Au(I) atom, formation of an aurophilic bond is impossible, however this conformational change provides insight into the Au(I)-Au(I) bond forming mechanism. Through LMCT into a nonbonding orbital, electron density is added to the Au(I) metal center and forces its observed bent structure.

Photophysics. Figure 9a depicts the steady-state absorption spectra of the synthesized compounds in THF. Generally, the transition energies were relatively large, with the molecules absorbing primarily in the UV region. A notable exception was for **Au$_2$-PhNO$_2$** and **Au$_2$-biTh**, which display distinctly lower energy bands centered at 395 and 375 nm, respectively. Extra caution was given to background corrections during acquisition of these absorption spectra, so the sharp rise in absorptivity at short wavelengths is real (i.e. attributed to molecular absorption and not the medium). The high energy absorption band (sub 350 nm) for these compounds displays a red-shifting trend when going from aryl donors of high IP to low IP. Namely, the long wavelength absorption onset increases in the sequence of **Au$_2$-Ph** (340 nm), **Au$_2$-Th** (365 nm), and **Au$_2$-PhNMe$_2$** (380 nm), which suggests that this feature is due to the LMCT absorption (*vide infra*). These LMCT states are further identified by comparison with the calculated spectra (Fig. 9b), which shows the results of 50 vertical excitations using CAM-B3LYP that are broadened with gaussian functions (FWHM = 50 nm). Compounds which display LMCT character in Figure 7 are in good agreement with experimental results, all showing long-wavelength absorption onsets at roughly 375 nm. This also serves as validation of the computational method, with CAM-B3LYP performing much better than other excited state methods. The only outlier here was Au$_2$-PhNO$_2$, which gave a 0.73 eV error compared to experimental results. However, further validation of the chosen density functional (CAM-B3LYP) is seen from the agreement in spectral shape between calculated and experimental results for all compounds. A more detailed comparison can be found in the SI, which also includes spectra calculated at the B3LYP level of theory.

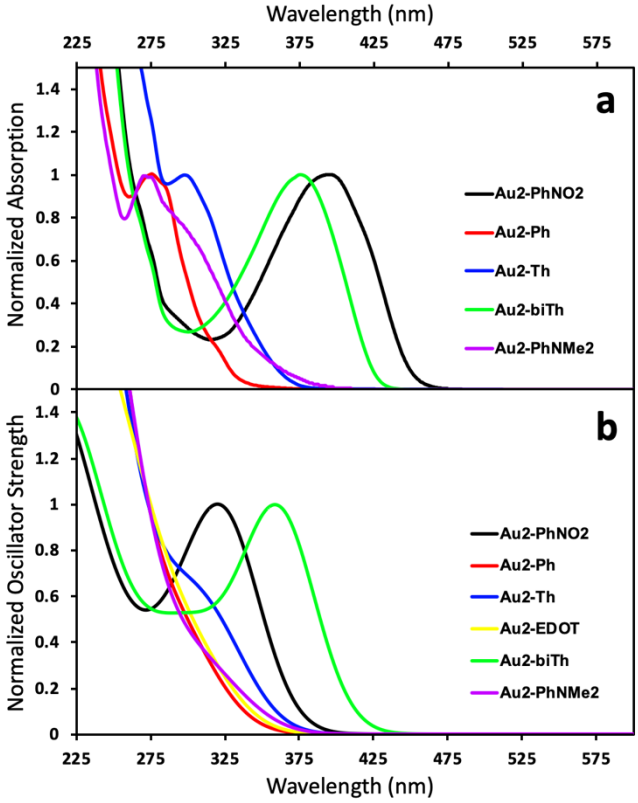

Figure 9. Normalized UV-Visible absorption spectra of digold triazolates. (**a**) Experimentally measured spectra of synthetic compounds collected in degassed THF. (**b**) Theoretical absorption spectra taken from the results of TDDFT calculations at the CAM-B3LYP level of theory comprised of a total of 50 excitations. Theoretical spectra are artificially broadened with gaussian functions (FWHM = 50 nm).

Figure 10 depicts emission spectra collected by exciting at 285 nm under an inert atmosphere and after exposure to air in all cases. Emission not quenched in air is from S_1 (fluorescence) and quenched emission originates from T_1 (phosphorescence). As such, **Au$_2$-PhNO$_2$** and **Au$_2$-biTh** are either strictly fluorescent or weakly phosphorescent, respectively (Figures 10a and 10d), with a fluorescence profile at much lower energy (λ_{max} = 475-500 nm) compared to other compounds that display fluorescence. The spectral shape and energetics of **Au$_2$-PhNO$_2$** is independent of excitation wavelength, differing only in relative emission intensity according to the varying absorptivity at different wavelengths. At higher electron donating strength, **Au$_2$-Th** displays only phosphorescence, with 100% of emission quenched upon exposure to air (Figure 11c). Other compounds of intermediate CT-character show dual emission, with varying relative contribution of phosphorescence to the total photoluminescence. With the exception of **Au$_2$-PhNO$_2$** and **Au$_2$-biTh**, the respective fluorescence and phosphorescence (when present) of each compound red shifts across the series of high IP aryl donors to low IP donors, showing typical

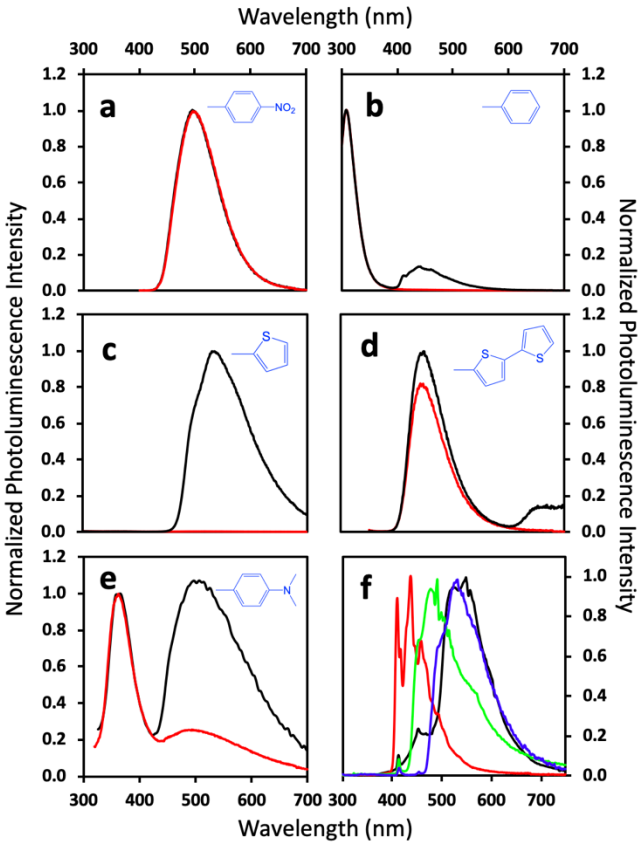

Figure 10. Normalized photoluminescence intensity in THF for (**a**) **Au₂-PhNO₂**, (**b**) **Au₂-Ph**, (**c**) **Au₂-Th**, (**d**) **Au₂-biTh**, and (**e**) **Au₂-PhNMe₂** where black lines indicate degassed conditions and red lines indicate air saturated conditions. (**f**) Emission at 77 K in Me-THF for **Au₂-PhNO₂** (—), **Au₂-Ph** (—), **Au₂-Th** (—), and **Au₂-PhNMe₂** (—).

LMCT emissive character. For stable compounds with reasonable phosphorescence, some vibronic structure is evident in this contribution to the total emission.

To further examine the emission spectra and attempt to elucidate evidence of Au(I)-Au(I) bond formation as predicted by the computational results, emission spectra were collected at 77 K in Me-THF (Figure 11f). All fluorescence of LMCT states quench at low temperature, meaning that the acquired spectra for **Ph**, **PhNMe₂**, and **Th** ligands are phosphorescence, while **Au₂-PhNO₂** shows the same fluorescence spectrum as shown in Figure 10a. It is obvious that the triplet energies decrease as the IP of the donor ligand decreases. At liquid nitrogen temperatures, a reduction in spectral broadening is expected to result in narrower lineshape in the component vibrational bands of the emission spectra. Interestingly, this was only observed for **Au₂-Ph**, which shows a spacing of 1500 cm^{-1} between the two most prominent peaks at 410 nm and 437 nm, corresponding to C=C stretching modes in aromatic compounds.

Subjected to the same spectroscopic analysis as the digold series, the results of steady-state spectroscopy on the monogold complex **Au₁-Th** shown in Figure 8b are depicted in Figure 11. Not surprising, considering emission of **Au₂-Th** is primarily phosphorescence, and previous work identified that the triplet state is characteristic of the ligand itself, the spectra for monogold **4,5-Au₁-Th** are very similar to those obtained for **Au₂-Th**.[46,47] Some differences between the mono and digold compounds is that the vibronic structure is better resolved for **Au₁-Th** compared to **Au₂-Th**, giving an energy spacing of 590 cm^{-1}, in the regime of bending and twisting motions. As evidence for excited state Au(I)-Au(I) bonding, inspection of the discrepancies between the degassed and air saturated conditions as shown in the SI revealed that there is still measurable fluorescence for **Au₂-Th** compared to **Au₁-Th**, however difficult to detect due to the fluorescence quantum yield being in competition with efficient intersystem crossing to the triplet state.

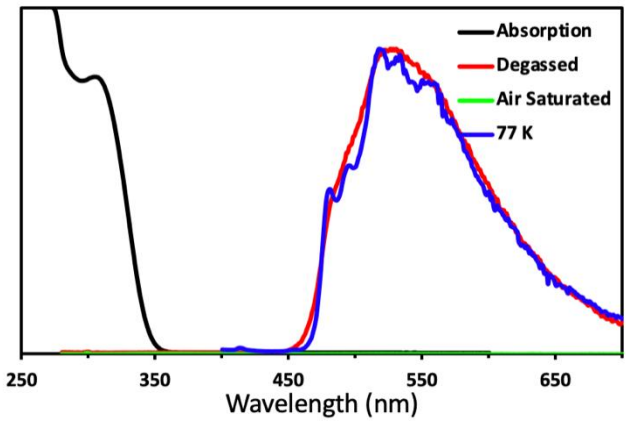

Figure 11. Normalized absorption (—) and emission (—, —, and —) spectra of monogold **4,5-Au₁-Th**. Spectra were collected in THF at room temperature and Me-THF at 77 K. The air-saturated spectrum was scaled to reflect relative emission intensity compared to degassed conditions.

DISCUSSION

Au₂-PhNO₂ and **Au₂-biTh** are distinct from the other compounds studied in several notable ways. TDHF and TDDFT results all indicate the S_1 for **Au₂-PhNO₂** and **Au₂-biTh** is primarily a localized excitation on the aryl triazolate ligand (Fig. 7). This is clearly evident from the CDD of this state, which actually shows a minor shift in electron density from the metal centers to the nitrophenyl and bithiophene moieties in the case of CAM-B3LYP. The electron withdrawing strength of the nitro group lowers the LUMO energy sufficiently to make the aryl ligand act as an acceptor rather than an electron donor. This property makes **Au₂-PhNO₂** an excellent control, where any excited state characteristics are not expected to originate from the effects of the Au(I) atoms. The geometry optimizations offer more evidence that **Au₂-PhNO₂** and **Au₂-biTh** do not exhibit excited state turn-on of aurophilic bonding. In both the ground state and excited state, the Au(I)-Au(I) distances remain beyond the limits of aurophilicity. Moreover, the emission spectra for **Au₂-PhNO₂** exhibits only fluorescence (Fig. 10). Exclusion of the Au(I) centers in the excited state wavefunction precludes the ability of the heavy atom effect to facilitate intersystem crossing. Without the aid of spin-orbit coupling, **Au₂-PhNO₂** and **Au₂-biTh** exclusively or predominately fluoresce, respectively, from a ligand-centered excited state. The results indicate the lower energy absorption band for **Au₂-PhNO₂** and **Au₂-biTh** is a localized excitation (LE) and the higher energy absorption band for the other complexes is a LMCT excitation to the Au(I) metal centers (Fig. 9). Regardless of which state is excited, **Au₂-PhNO₂** and **Au₂-biTh** always emit from the LE, due to Kasha's rule.

A more complicated interplay between the Au(I) atoms and the excited state characteristics were expected of the remaining compounds. From the computational results, S_1 for all the other compounds display obvious CT-character with charge density shifting towards the metal centers (Fig. 7). For a given computational method, the CDDs of this LMCT state appear fundamentally the same. However, observed as a red-shift in the electronic spectra across the series of synthesized compounds (Fig. 9), the excitation energy decreases for smaller donor IPs due to the raising of the HOMO energy level where the electron-hole for these excited states is located. This effect is further exemplified in the calculated excitation energies (Table 1) decreasing with decreasing IP, with the exception of **Au_2-$PhNO_2$** and **Au_2-biTh**, which do not fit this trend due to the localization of the excited state on the aryl component.

Of particular interest is how the CDDs display a bonding type MO between the Au(I) atoms in the excited state, regardless of computational method. At a minimum, this indicates that the two Au(I) atoms have shared electron density after photoexcitation. Evidence of the metal contribution to the excited state is seen in the emission spectra (Fig. 10), where fluorescence is sharp and intense, as is typical of aurophilic emission.[18–21] Similar to how **Au_2-$PhNO_2$** and **Au_2-biTh** did not display appreciable phosphorescence because a lack of augmented spin-orbit coupling, the added contribution from the metal centers of the remaining compounds gives rise to phosphorescence. Moreover, as ligand donor strength is increased, the apparent contribution of the phosphorescence increases. These data demonstrate empirically that the "turn-on" of aurophilicity in the excited state is achievable by varying the HOMO energy level of a neighboring chromophore without lowering its associated LUMO energy below that of the Au(I) electron acceptor.

An equally important result from this work is the structural change upon relaxing this excited state through different computational methods. Because HF implements the mean-field approximation to combat the problem of correlated electrons, dispersive forces are absent from the energetics. Even for ground states, HF cannot model aurophilic bonding, considering that dispersion is a fundamental component of aurophilicity theory. In contrast, methods that include Coulombic correlation display contractions in the Au(I)-Au(I) distance that are well within the cutoff for accepted aurophilic character. For methods that better model CT excited states (CAM-B3LYP), the aurophilic bonding is strengthened and bolsters the hypothesis that charge transfer to the Au(I) metal centers augment Van der Waals to facilitate aurophilic bonding.

The bond angle decrease between the N-Au-P atoms is another structural change to consider. Typically, aurophilic bonding between two linear Au(I) complexes occurs with the linear bonding axes of the individual metal centers being orthogonal with respect to one another.[2,48] The structure of the compounds studied here precludes such an interaction without excessive distortion. Unable to approach orthogonally the complex distorts through the N-Au-P angle to accommodate. This appears to be an inherent property of the Au(I) metal center in the LMCT state, since the single Au(I) ion complex **Au_1-Th** also exhibits the distortion. Ultimately, changing from linear to a trigonal planar geometry allows for interaction with the other Au(I) metal center in the digold compounds to form the new bond. CT character favoring one metal center over the other is likely the reason the angle distortion only occurs for the N-bound Au(I) ion.

CONCLUSION

A series of iClick synthesized digold compounds that exhibit a range of aryl donor-motif chromophores with different IPs were studied computationally and spectroscopically. At ~3.5-3.7 Å from each other and enforced by a semi-supported architecture, the sum of the Van der Waals radii for each complex in the ground-state is beyond the accepted value for an aurophilic bond. Vertical excitation calculations reveal compounds with aryl ligands of sufficiently low IP exhibit charge transfer character to the Au(I) metal centers. Geometry optimizations of the excited states that include Coulombic correlation exhibit bond contraction and excited-state activation of aurophilicity. Providing evidence for an excited state aurophilic bond, an increase in triplet quantum yield correlates with CT to Au(I). Case in point is the example of **Au_2-$PhNO_2$** and **Au_2-biTh** that do not exhibit phosphorescence and their computed S_1 states are ligand localized and do not exhibit Au(I)-Au(I) contraction. In addition, unable to partner with an adjacent gold ion, the monogold complexes exhibit CT resulting in a bending in the N-Au-P atoms, thus suggesting a possible mechanism for the turn-on of aurophilcity in this series of complexes. As such, it is now possible to choose donor chromophores such that excited-state aurophilicity is either on or off, and simple choice of donor IP can tune the extent of intersystem crossing and thus the magnitude of aurophilicity in the excited state. Since aurophilic bonds are often unstable in solution, this new level of control may prove useful in light induced self-assembly of supramolecular structures, device fabrication, bio sensing, molecular switches, and general processability.[49]

EXPERIMENTAL

Unless specified otherwise, all manipulations were performed under an inert atmosphere using standard Schlenk or glove-box techniques. Pentane, methylene chloride (DCM), diethyl ether, and tetrahydrofuran (THF) were degassed by sparging with high purity argon, and were dried using a GlassContour drying column. Methanol was dried over anhydrous copper(II)sulfate, distilled and stored over 4 Å molecular sieves; chloroform-*d* (Cambridge Isotopes) was dried over calcium hydride, distilled, and stored over 4 Å molecular sieves. ^{1}H, ^{13}C{^{1}H}, and ^{31}P{^{1}H} NMR spectra were acquired on a Varian Mercury 300 MHz, a Bruker 400 MHz, an Inova 500 MHz, or a Varian Agilent 600 MHz spectrometer. 2D NMR spectra were obtained on a Bruker 400 MHz, an Inova 500 MHz or a Varian Agilent 600 MHz spectrometer. Chemical shifts are reported in δ (ppm). For ^{1}H and ^{13}C NMR spectra, the residual solvent peaks were used as an internal reference standard, while ^{31}P{^{1}H} spectra were referenced to an 85% phosphoric acid external standard (0 ppm). Data are reported as follows: chemical shift, multiplicity (s = singlet, d = doublet, t = triplet, q = quartet, dd = doublet of doublets, m = multiplet, b = broad) and integration. ESI-MS analysis were performed by Manasi Kamat, Subhradeep Bhar, and Atiye Ahmadi at Mass Spectrometry Research and Education Center, the Chemistry Department. Elemental analyses were performed at the CENTC Elemental Analysis facility at University of Rochester, NY. The following materials were purchased and used

ACS Paragon Plus Environment

as received: chlorotriphenylphosphinegold(I) (PPh_3AuCl) (Acros), 2-ethynylthiophene (Accela), 4-ethynyl-N,N-dimethylaniline (Sigma-Aldrich), 2,2-bithiophene (Oakwood Chemical), sodium azide (NaN_3) (Sigma-Aldrich). The following were prepared by literature methods: PPh_3AuN_3,[50] $PPh_3AuC{\equiv}CPh$,[51] $PPh_3AuC{\equiv}CC_6H_4NO_2$,[52] $Br(C_4H_2S)(C_4H_3S)$,[53] $PPh_3AuC{\equiv}C(C_4H_2S)(C_4H_3S)$,[54] (**$Au_2$-Ph**),[37] (**$Au_2$-$PhNO_2$**).[38]

General procedure for the synthesis of triphenylphoshinegold(I) acetylides (**$PPh_3AuC{\equiv}CTh$, $PPh_3AuC{\equiv}CPhNMe_2$**). H-C≡C-R (R = Th, $PhNMe_2$) (0.5 mmol), PPh_3Au-Cl (0.5 mmol), and K_2CO_3 (1.5 mmol) were added into a solution mixture of 4 mL THF and 1 mL MeOH. The solution was stirred in the dark for 24 h. Water was added and the compound was extracted with chloroform, then dried over anhydrous $MgSO_4$. Crystals were grown through pentane diffusion into a methylene chloride solution of gold acetylide at -25 °C.

General Procedure for the synthesis of digold-triazolate (**Au_2-Th**, **Au_2-$PhNMe_2$**, **Au_2-biTh**). PPh_3Au-C≡C-R (R = Th, $PhNMe_2$, biTh) (0.05 mmol), and PPh_3Au-N_3 (0.05 mmol) were dissolved into 2 mL of $CDCl_3$. The solution was added to a J. Young tube and the product formation was monitored via ^1H and ^{31}P NMR spectroscopy. The reaction was stopped after 1 h and the solvent was removed in *vacuo*. Crystals were grown through pentane diffusion into a methylene chloride solution of the triazolate at -25 °C.

$PPh_3AuC{\equiv}CTh$. 74.4 % Yield (0.37 mmol, 209.6 mg). ^1H NMR (500 MHz, $CDCl_3$): δ 6.89 (dd, $^3J_{HH}$ = 3.5, 5.1 Hz, 1H, C_5-H), 7.08 (dd, $^3J_{HH}$ = 5.2 Hz, $^4J_{HH}$ = 1.2 Hz, 1H, C_4-H), 7.15 (dd, $^3J_{HH}$ = 3.7 Hz, $^3J_{HH}$ = 1.3 Hz, 1H, C_6-H), 7.43-7.56 (m, 15H, aromatic). $^{13}C\{^1H\}$ NMR (indirect detection through ^1H-^{13}C gHMBC and ^1H-^{13}C gHSQC (126 MHz, $CDCl_3$)): δ 125.1 (C_4), 125.2 (C_3), 126.5 (C_5), 129.1 (d, $^4J_{CP}$ = 11 Hz, C_{10}), 129.6 (d, $^1J_{CP}$ = 56 Hz, C_7), 131.1 (C_6), 131.5 (d, $^3J_{CP}$ = 3 Hz, C_9), 134.3 (d, $^2J_{CP}$ = 14 Hz, C_8). $^{31}P\{^1H\}$ NMR (121 MHz, $CDCl_3$): δ 42.52. ESI-MS: m/z calculated for $C_{24}H_{18}AuPS$ $[M+Na]^+$ 589.0430, found 589.0408. Anal. Calcd. for $C_{24}H_{18}AuPS$: C, 50.89; H, 3.20. Found: C, 50.60; H, 3.11; N, -0.23.

$PPh_3AuC{\equiv}CPhNMe_2$. 62.3 % Yield (0.31 mmol, 187.9 mg). ^1H NMR (500 MHz, $CDCl_3$): δ 2.91 (s, 6H, C_7-H), 6.57 (d, $^3J_{HH}$ = 8.4 Hz, 2H, C_5-H), 7.35-7.55 (m, 17H, C_4-H and aromatic). $^{13}C\{^1H\}$ NMR (indirect detection through ^1H-^{13}C gHMBC and ^1H-^{13}C gHSQC (126 MHz, $CDCl_3$)): δ 40.3 (C_7), 111.8 (C_5), 112.1 (C_3), 129.1 (d, $^4J_{CP}$ = 11 Hz, C_{11}), 130.0 (d, $^1J_{CP}$ = 55 Hz, C_8), 131.4 (d, $^3J_{CP}$ = 2 Hz, C_{10}), 133.4 (C_4), 134.3 (d, $^2J_{CP}$ = 14 Hz, C_9), 149.2 (C_6). $^{31}P\{^1H\}$ NMR (121 MHz, $CDCl_3$): δ 42.52. ESI-MS: m/z calculated for $C_{28}H_{25}AuNP$ $[M+H]^+$ 604.1468, found 604.1438.

Au_2-Th. 93.8% Yield (0.047 mmol, 50.1 mg). ^1H NMR (500 MHz, $CDCl_3$): δ 6.85-6.90 (m, 2H, C_5-H and C_6-H), 7.12-7.21 (m, 12H, C_9-H and C_{13}-H), 7.28-7.30 (m, 6H, C_{10}-H and C_{14}-H), 7.38-7.43 (m, 12H, C_8-H and C_{12}-H), 7.60-7.62 (m, 1H, C_4-H). $^{13}C\{^1H\}$ NMR (indirect detection through ^1H-^{13}C gHMBC and ^1H-^{13}C gHSQC (126 MHz, $CDCl_3$)): δ 120.7 (C_4), 121.1 (C_5), 127.1 (C_6), 129.1 (d, $^3J_{CP}$ = 11 Hz, C_9 and C_{13}), 131.5 (d, $^4J_{CP}$ = 12 Hz, C_{10} and C_{14}), 134.3 (d, $^2J_{CP}$ = 14 Hz, C_8 and C_{12}), 140.2 (C_3). $^{31}P\{^1H\}$ NMR (121 MHz, $CDCl_3$): δ 44.59 (s, P1), 31.50 (s, P2). ESI-MS: m/z calculated for $C_{42}H_{33}Au_2N_3P_2S$ $[M+H]^+$ 1068.1280, found 1068.1252.

Au_2-$PhNMe_2$. 92.5 % Yield (0.046 mmol, 51.1 mg). ^1H NMR (500 MHz, $CDCl_3$): δ 2.89 (s, 6H, C_7-H), 6.69 (d, $^3J_{HH}$ = 8.3 Hz, 2H, C_5-H), 7.18-7.21 (m, 12H, C_{10}-H and C_{14}-H), 7.33-7.35 (m, 6H, C_{11}-H and C_{15}-H), 7.43-7.47 (m, 12H, C_9-H and C_{13}-H), 8.24 (d, $^3J_{HH}$ = 8.2 Hz, 2H, C_4-H). $^1C\{^1H\}$ NMR (indirect detection through ^1H-^{13}C gHMBC and ^1H-^{13}C gHSQC (126 MHz, $CDCl_3$)): δ 41.0 (C_7), 112.8 (C_5), 126.1 (C_3), 127.3 (C_4), 129.0 (d, $^3J_{CP}$ = 11 Hz, C_{10} and C_{14}), 131.4 (C_{11} and C_{15}), 134.2 (d, $^2J_{CP}$ = 14 Hz, C_9 and C_{13}), 136.5 (C_8 and C_{12}), 149.2 (C_6), 151.7 (C_2). $^{31}P\{^1H\}$ NMR (121 MHz, $CDCl_3$): δ 44.61 (s, P1), 31.17 (s, P2). ESI-MS: m/z calculated for $C_{46}H_{40}Au_2N_4P_2$ $[M+H]^+$ 1105.2138, found 1105.2104.

Au_2-biTh. 95.3% Yield (0.089 mmol, 102 mg). ^1H-NMR (600MHz, $CDCl_3$), δ (ppm): 6.91 (dd, $^3J_{HH}$ = 3.5 Hz, $^4J_{HH}$ = 1.0 Hz, 1H, C_8-H), 6.95 (dd, $^3J_{HH}$ = 5.0 Hz, $^3J_{HH}$ = 3.6 Hz, 1H, C_9-H), 7.09 (d, $^3J_{HH}$ = 3.7 Hz, 1H, C_5-H), 7.12 (d, $^3J_{HH}$ = 4.8 Hz, 1H, C_{10}-H), 7.24-7.38 (m, 12H, C_{13}-H and C_{17}-H), 7.40-7.49 (m, 6H, C_{14}-H and C_{18}-H), 7.48-7.60 (m, 12H, C_{12}-H and C_{16}-H), 7.61 (d, $^3J_{HH}$ = 3.7 Hz, 1H, C_4-H).$^{13}C\{^1H\}$ NMR (indirect detection through ^1H-^{13}C gHMBC and ^1H-^{13}C gHSQC) (600 MHz, $CDCl_3$), δ (ppm): 121.78 (C_4), 122.42 (C_8), 122.94 (C_{10}), 124.25 (C_5), 127.41 (C_9), 128.48 (d, $^1J_{CP}$ = 12 Hz, C_{11} and C_{15}), 129.12 (d, $^3J_{CP}$ = 11 Hz, C_{13} and C_{17}), 131.56 (m, C_{14} and C_{18}), 132.07 (C_6), 134.25 (d, $^2J_{CP}$ = 14 Hz, C_{12} and C_{16}), 138.80 (C_7), 145.56 (C_2). $^{31}P\{^1H\}$ NMR (242.9 MHz, $CDCl_3$), δ (ppm): 44.58 (s, P_1), 31.18 (s, P_2). ESI-MS: m/z calculated for $C_{46}H_{35}Au_2N_3P_2S_2$ $[M+H]^+$ 1150.1157, found 1150.1122.

4,5-Au_1-Th. H-C≡C-Th (0.05 mmol) and PPh_3Au-N_3 (0.05 mmol) were added into 2 mL of DCM. The solution was stirred in the dark for 5 h then solvents was removed *in vacuo*. Crystals were grown through pentane diffusion into a methylene chloride solution of the triazolate at -25 °C. 91.1% Yield (0.046 mmol, 27.77 mg). ^1H NMR (400 MHz, $CDCl_3$): δ 7.00 (dd, $^3J_{HH}$ = 3.5, 5.0 Hz, 1H, C_5-H), 7.06 (dd, $^3J_{HH}$ = 5.0 Hz, $^4J_{HH}$ = 1.2 Hz, 1H, C_4-H), 7.74 (dd, $^3J_{HH}$ = 3.6 Hz, $^4J_{HH}$ = 1.2 Hz, 1H, C_6-H), 7.49-7.63 (m, 15H, C_8-H, C_9-H and C_{10}-H). $^{13}C\{^1H\}$ NMR (indirect detection through ^1H-^{13}C gHMBC and ^1H-^{13}C gHSQC (101 MHz, $CDCl_3$)): δ 122.1 (C_4), 122.6 (C_6), 127.4 (C_5), 129.3 (d, $^3J_{CP}$ = 11 Hz, C_9), 129.7 (d, $^1J_{CP}$ = 55 Hz, C_7), 131.7 (d, $^4J_{CP}$ = 2 Hz, C_{10}), 134.3 (d, $^2J_{CP}$ = 13 Hz, C_8), 137.8 (C_8), 148.1 (C_9). $^{31}P\{^1H\}$ NMR (161 MHz, $CDCl_3$): δ 43.50. ESI-MS: m/z calculated for $C_{24}H_{19}AuN_3PS$ $[M+H]^+$ 610.0781, found 610.0762.

Computational Methods. All calculations were done in Gaussian 16 (Revision B.01) on a home-built 64-core local machine.[45] For all methods, a 6-31G(d) basis set was used for C, H, N, and O; a 6-31+G(d) basis set was used for P; and the SDD basis set was used for Au as it is employed in the software package.[55] This corresponds to the Stuttgart-Dresden pseudopotential, ECP60MWB, which uses an intermediate treatment of relativistic effects for the effective core potential.[56] This way relativistic effects are derived from the basis set, and not from the more computationally expensive Dirac equation. For all compounds, triphenyl phosphine ligands were reduced to trimethyl phosphines to reduce computational costs. Validation of this simplification can be found in the SI. A total of 50 vertical excitations were used to generate the calculated absorption spectra, whereas excited state geometry optimizations used only a single excitation. In all cases, symmetry constraints were turned off, an ultrafine integration grid was used, and calculations were done in the gas phase. NBO analysis was done using the Multiwfn software package.[57]

Spectroscopy. Samples for spectroscopic analysis were prepared in an inert atmosphere glovebox and kept isolated from light. A 1 cm path length quartz cell was used for these measurements with THF that was dried and purified by an MBraun MB-SPS-800 solvent purification system. Steady-state UV-Vis absorption spectra were recorded on Shimadzu UV-1800 dual-beam spectrophotometer and emission spectra were collected with an Edinburgh FLS1000 photoluminescence spectrometer where an optical density of 0.6 was used at the excitation wavelength. Low temperature measurements were made with the aid of liquid N_2 poured into a dewar with glass windows.

ASSOCIATED CONTENT

Synthetic details, NMR spectra, photophysical characterization data, computational details. This material is available free of charge via the Internet at http://pubs.acs.org.

AUTHOR INFORMATION

Corresponding Author(s)

* veige@chem.ufl.edu
* kirk.schanze@utsa.edu

Author Contributions

All authors contributed to the writing of this manuscript. All authors have given approval to the final version of the manuscript.

Funding Sources

Research supported by the U.S. Department of Energy, Office of Basic Energy Sciences, Division of Materials Sciences and Engineering under Award DE-SC0020008. The UF Mass Spectrometry Research and Education Center (NIH S10 OD021758-01A1) are thanked for acquisition of mass spectrometry data. K.A.A acknowledges the NSF (CHE-0821346) for the purchase of X-ray equipment.

REFERENCES

(1) Schmidbaur, H.; Wohlleben, A.; Wagner, F.; Orama, O.; Huttner, G. Gold-Komplexe von Diphosphinomethanen, I. Synthese Und Kristallstruktur Zweikerniger Gold(I)-Verbindungen. *Chem. Ber.* **1977**, *110*, 1748–1754.

(2) Schmidbaur, H. The Aurophilicity Phenomenon: A Decade of Experimental Findings, Theoretical Concepts and Emerging Applications. *Gold Bull.* **2000**, *33*, 3–10.

(3) Schmidbaur, H.; Schier, A. Aurophilic Interactions as a Subject of Current Research: An up-Date. *Chem. Soc. Rev.* **2012**, *41*, 370–412.

(4) Schmidbaur, H.; Dziwok, K.; Grohmann, A.; Müller, G. Further Evidence for Attractive Interactions between Gold(I) Centers in Binuclear Complexes. *Chem. Ber.* **1989**, *122*, 893–895.

(5) Pyykkö, P. Theoretical Chemistry of Gold. *Angew. Chemie Int. Ed.* **2004**, *43*, 4412–4456.

(6) Pyykkö, P. Strong Closed-Shell Interactions in Inorganic Chemistry. *Chem. Rev.* **1997**, *97*, 597–636.

(7) Uson, R. A Review of: "The Chemistry of Gold. R.J. Puddephatt. Topics in Inorganic and General Chemistry-Monograph 16, Edited by R. J. H. Clark. Elsevier, Amsterdam, Oxford, New York, 1978, 274 p. $49.75." *Synth. React. Inorg. Met. Chem.* **1978**, *8*, 503–504.

(8) Scherbaum, F.; Grohmann, A.; Huber, B.; Krüger, C.; Schmidbaur, H. "Aurophilicity" as a Consequence of Relativistic Effects: The Hexakis (Triphenyl phosphaneaurio)Methane Dication $[(Ph_3PAu)_6C]^{2+}$. *Angew. Chemie Int. Ed.* **1988**, *27*, 1544–1546.

(9) Schmidbaur, H.; Graf, W.; Müller, G. Weak Intramolecular Bonding Relationships: The Conformation-Determining Attractive Interaction between Gold(I) Centers. *Angew. Chemie Int. Ed.* **1988**, *27*, 417–419.

(10) Runeberg, N.; Schütz, M.; Werner, H.-J. The Aurophilic Attraction as Interpreted by Local Correlation Methods. *J. Chem. Phys.* **1999**, *110*, 7210–7215.

(11) Pyykko, P. Relativistic Effects in Structural Chemistry. *Chem. Rev.* **1988**, *88*, 563–594.

(12) Pyykkö, P. Relativistic Effects on Periodic Trends BT - The Effects of Relativity in Atoms, Molecules, and the Solid State; Wilson, S., Grant, I. P., Gyorffy, B. L., Eds.; Springer US: Boston, MA, 1991; pp 1–13.

(13) Pyykkö, P. Theoretical Chemistry of Gold. III. *Chem. Soc. Rev.* **2008**, *37*, 1967–1997.

(14) Schwerdtfeger, P. Relativistic Effects in Properties of Gold. *Heteroat. Chem.* **2002**, *13*, 578–584.

(15) Dedieu, A.; Hoffmann, R. Platinum(0)-Platinum(0) Dimers. Bonding Relationships in a d10-d10 System. *J. Am. Chem. Soc.* **1978**, *100*, 2074–2079.

(16) Mehrotra, P. K.; Hoffmann, R. Copper(I)-Copper(I) Interactions. Bonding Relationships in d^{10}-d^{10} Systems. *Inorg. Chem.* **1978**, *17*, 2187–2189.

(17) Li, J.; Pyykkö, P. Relativistic Pseudo-Potential Analysis of the Weak Au(I)…Au(I) Attraction. *Chem. Phys. Lett.* **1992**, *197*, 586–590.

(18) Yam, V. W.-W.; Au, V. K.-M.; Leung, S. Y.-L. Light-Emitting Self-Assembled Materials Based on d^8 and d^{10} Transition Metal Complexes. *Chem. Rev.* **2015**, *115*, 7589–7728.

(19) Coker, N. L.; Krause Bauer, J. A.; Elder, R. C. Emission Energy Correlates with Inverse of Gold–Gold Distance for Various $[Au(SCN)_2]^-$ Salts. *J. Am. Chem. Soc.* **2004**, *126*, 12–13.

(20) Rawashdeh-Omary, M. A.; Omary, M. A.; Patterson, H. H.; Fackler, J. P. Excited-State Interactions for $[Au(CN)^{2-}]_n$ and $[Ag(CN)^{2-}]_n$ Oligomers in Solution. Formation of Luminescent Gold–Gold Bonded Excimers and Exciplexes. *J. Am. Chem. Soc.* **2001**, *123*, 11237–11247.

(21) Forward, J. M.; Bohmann, D.; Fackler, J. P.; Staples, R. J. Luminescence Studies of Gold(I) Thiolate Complexes. *Inorg. Chem.* **1995**, *34*, 6330–6336.

(22) Tang, S. S.; Chang, C.-P.; Lin, I. J. B.; Liou, L.-S.; Wang, J.-C. Molecular Aggregation of Annular Dinuclear Gold(I) Compounds Containing Bridging Diphosphine and Dithiolate Ligands. *Inorg. Chem.* **1997**, *36*, 2294–2300.

(23) Jiang, X.-F.; Hau, F. K.-W.; Sun, Q.-F.; Yu, S.-Y.; Yam, V. W.-W. From {AuI···AuI}-Coupled Cages to the Cage-Built 2-D {AuI···AuI} Arrays: AuI···AuI Bonding Interaction Driven Self-Assembly and Their AgI Sensing and Photo-Switchable Behavior. *J. Am. Chem. Soc.* **2014**, *136*, 10921–10929.

(24) Lu, X.; Yavuz, M. S.; Tuan, H.-Y.; Korgel, B. A.; Xia, Y. Ultrathin Gold Nanowires Can Be Obtained by Reducing Polymeric Strands of Oleylamine–AuCl Complexes Formed via Aurophilic Interaction. *J. Am. Chem. Soc.* **2008**, *130*, 8900–8901.

(25) Koshevoy, I. O.; Smirnova, E. S.; Haukka, M.; Laguna, A.; Chueca, J. C.; Pakkanen, T. A.; Tunik, S. P.; Ospino, I.; Crespo, O. Synthesis, Structural Characterization, Photophysical Properties and Theoretical Analysis of Gold(I) Thiolate-Phosphine Complexes. *Dalt. Trans.* **2011**, *40*, 7412–7422.

(26) Ni, W.-X.; Li, M.; Zheng, J.; Zhan, S.-Z.; Qiu, Y.-M.; Ng, S. W.; Li, D. Approaching White-Light Emission from a Phosphorescent Trinuclear Gold(I) Cluster by Modulating Its Aggregation Behavior. *Angew. Chemie Int. Ed.* **2013**, *52*, 13472–13476.

(27) Earl, L. D.; Nagle, J. K.; Wolf, M. O. Tuning the Extended Structure and Electronic Properties of Gold(I) Thienyl Pyrazolates. *Inorg. Chem.* **2014**, *53*, 7106–7117.

(28) Beto, C. C.; Zeman, C. J.; Yang, Y.; Bullock, J. D.; Holt, E. D.; Kane, A. Q.; Makal, T. A.; Yang, X.; Ghibiriga, I.; Schanze, K. S.; et al. An Application Exploiting Aurophilic Bonding and iClick to Produce White Light Emitting Materials. *Inorg. Chem.* **2020**, *59*, 1893-1904.

(29) Mihaly, J. J.; Stewart, D. J.; Grusenmeyer, T. A.; Phillips, A. T.; Haley, J. E.; Zeller, M.; Gray, T. G. Photophysical Properties of Organogold(I) Complexes Bearing a Benzothiazole-2,7-Fluorenyl Moiety: Selection of Ancillary Ligand Influences White Light Emission. *Dalt. Trans.* **2019**, *48*, 15917–15927.

(30) Kim, K. H.; Kim, J. G.; Nozawa, S.; Sato, T.; Oang, K. Y.; Kim, T. W.; Ki, H.; Jo, J.; Park, S.; Song, C.; et al. Direct Observation of Bond Formation in Solution with Femtosecond X-Ray Scattering. *Nature* **2015**, *518*, 385–389.

(31) Penney, A. A.; Sizov, V. V; Grachova, E. V; Krupenya, D. V; Gurzhiy, V. V; Starova, G. L.; Tunik, S. P. Aurophilicity in Action: Fine-Tuning the Gold(I)–Gold(I) Distance in the Excited State To Modulate the Emission in a Series of Dinuclear Homoleptic Gold(I)–NHC Complexes. *Inorg. Chem.* **2016**, *55*, 4720–4732.

(32) Baron, M.; Tubaro, C.; Biffis, A.; Basato, M.; Graiff, C.; Poater, A.; Cavallo, L.; Armaroli, N.; Accorsi, G. Blue-Emitting Dinuclear N-Heterocyclic Dicarbene Gold(I) Complex Featuring a Nearly Unit Quantum Yield. *Inorg. Chem.* **2012**, *51*, 1778–1784.

(33) Latouche, C.; Lin, Y.-R.; Tobon, Y.; Furet, E.; Saillard, J.-Y.; Liu, C.-W.; Boucekkine, A. Au–Au Chemical Bonding Induced by UV Irradiation of Dinuclear Gold(I) Complexes: A Computational Study with Experimental Evidence. *Phys. Chem. Chem. Phys.* **2014**, *16*, 25840–25845.

(34) Brown-Xu, S. E.; Kelley, M. S. J.; Fransted, K. A.; Chakraborty, A.; Schatz, G. C.; Castellano, F. N.; Chen, L. X. Tunable Excited-State Properties and Dynamics as a Function of Pt–Pt Distance in Pyrazolate-Bridged Pt(II) Dimers. *J. Phys. Chem. A* **2016**, *120*, 543–550.

(35) Kim, P.; Kelley, M. S.; Chakraborty, A.; Wong, N. L.; Van Duyne, R. P.; Schatz, G. C.; Castellano, F. N.; Chen, L. X. Coherent Vibrational Wavepacket Dynamics in Platinum(II) Dimers and Their Implications. *J. Phys. Chem. C* **2018**, *122*, 14195–14204.

(36) Yang, X.; Wang, S.; Ghiviriga, I.; Abboud, K. A.; Veige, A. S. Organogold Oligomers: Exploiting iClick and Aurophilic Cluster Formation to Prepare Solution Stable Au4 Repeating Units. *Dalt. Trans.* **2015**, *44*, 11437–11443.

(37) Del Castillo, T. J.; Sarkar, S.; Abboud, K. A.; Veige, A. S. 1,3-Dipolar Cycloaddition between a Metal–Azide (Ph_3PAuN_3) and a Metal–Acetylide ($Ph_3PAuC{\equiv}CPh$): An Inorganic Version of a Click Reaction. *Dalt. Trans.* **2011**, *40*, 8140–8144.

(38) Powers, A. R.; Ghiviriga, I.; Abboud, K. A.; Veige, A. S. Au-iClick Mirrors the Mechanism of Copper Catalyzed Azide–Alkyne Cycloaddition (CuAAC). *Dalt. Trans.* **2015**, *44*, 14747–14752.

(39) Møller, C.; Plesset, M. S. Note on an Approximation Treatment for Many-Electron Systems. *Phys. Rev.* **1934**, *46*, 618–622.

(40) Becke, A. D. Density-Functional Exchange-Energy Approximation with Correct Asymptotic Behavior. *Phys. Rev. A* **1988**, *38*, 3098–3100.

(41) Becke, A. D. Density-functional Thermochemistry. III. The Role of Exact Exchange. *J. Chem. Phys.* **1993**, *98*, 5648–5652.

(42) Lee, C.; Yang, W.; Parr, R. G. Development of the Colle-Salvetti Correlation-Energy Formula into a Functional of the Electron Density. *Phys. Rev. B* **1988**, *37*, 785–789.

(43) Yanai, T.; Tew, D. P.; Handy, N. C. A New Hybrid Exchange–Correlation Functional Using the Coulomb-Attenuating Method (CAM-B3LYP). *Chem. Phys. Lett.* **2004**, *393*, 51–57.

(44) Foresman, J. B.; Head-Gordon, M.; Pople, J. A.; Frisch, M. J. Toward a Systematic Molecular Orbital Theory for Excited States. *J. Phys. Chem.* **1992**, *96*, 135–149.

(45) Frisch, M. J.; Trucks, G. W.; Schlegel, H. B.; Scuseria, G. E.; Robb, M. A.; Cheeseman, J. R.; Scalmani, G.; Barone, V.; Mennucci, B.; Petersson, G. A.; et al. Gaussian 09, Revision B.01. *Gaussian 09, Revision B.01, Gaussian, Inc., Wallingford CT*. Wallingford CT 2009.

(46) Lu, W.; Kwok, W.-M.; Ma, C.; Chan, C. T.-L.; Zhu, M.-X.; Che, C.-M. Organic Triplet Excited States of Gold(I) Complexes with Oligo(o- or m-Phenyleneethynylene) Ligands: Conjunction of Steady-State and Time-Resolved Spectroscopic Studies on Exciton Delocalization and Emission Pathways. *J. Am. Chem. Soc.* **2011**, *133*, 14120–14135.

(47) Hsu, C.-C.; Lin, C.-C.; Chou, P.-T.; Lai, C.-H.; Hsu, C.-W.; Lin, C.-H.; Chi, Y. Harvesting Highly Electronically Excited Energy to Triplet Manifolds: State-Dependent

Intersystem Crossing Rate in Os(II) and Ag(I) Complexes. *J. Am. Chem. Soc.* **2012**, *134*, 7715–7724.

(48) Schmidbaur, H.; Schier, A. A Briefing on Aurophilicity. *Chem. Soc. Rev.* **2008**, *37*, 1931–1951.

(49) Wu, Z.; Du, Y.; Liu, J.; Yao, Q.; Chen, T.; Cao, Y.; Zhang, H.; Xie, J. Aurophilic Interactions in the Self-Assembly of Gold Nanoclusters into Nanoribbons with Enhanced Luminescence. *Angew. Chemie Int. Ed.* **2019**, *58*, 8139–8144.

(50) Kolb, H. C.; Finn, M. G.; Sharpless, K. B. Click Chemistry: Diverse Chemical Function from a Few Good Reactions. *Angew. Chemie Int. Ed.* **2001**, *40*, 2004–2021.

(51) Huisgen, R. *1,3-Dipolar Cycloaddition Chemistry*, A.; Padwa: New York, 1984.

(52) Whittall, I. R.; Humphrey, M. G.; Houbrechts, S.; Persoons, A.; Hockless, D. C. R. Organometallic Complexes for Nonlinear Optics. 8.1 Syntheses and Molecular Quadratic Hyperpolarizabilities of Systematically Varied (Triphenylphosphine)Gold σ-Arylacetylides: X-Ray Crystal Structures of Au(C:CR)(PPh_3) (R = 4-$C_6H_4NO_2$, 4,4'-$C_6H_4C_6H_4NO_2$). *Organometallics* **1996**, *15*, 5738–5745.

(53) Frigoli, M.; Moustrou, C.; Samat, A.; Guglielmetti, R. Photomodulable Materials. Synthesis and Properties of Photochromic 3H-Naphtho[2,1-b]Pyrans Linked to Thiophene Units via an Acetylenic Junction. *Helv. Chim. Acta* **2000**, *83*, 3043–3052.

(54) Li, P.; Ahrens, B.; Choi, K.-H.; Khan, M. S.; Raithby, P. R.; Wilson, P. J.; Wong, W.-Y. Metal–Metal and Ligand–Ligand Interactions in Gold Poly-Yne Systems. *CrystEngComm* **2002**, *4*, 405–412.

(55) Ditchfield, R.; Hehre, W. J.; Pople, J. A. Self-Consistent Molecular-Orbital Methods. IX. An Extended Gaussian-Type Basis for Molecular-Orbital Studies of Organic Molecules. *J. Chem. Phys.* **1971**, *54*, 724–728.

(56) Andrae, D.; Häußermann, U.; Dolg, M.; Stoll, H.; Preuß, H. Energy-Adjustedab Initio Pseudopotentials for the Second and Third Row Transition Elements. *Theor. Chim. Acta* **1990**, *77*, 123–141.

(57) Lu, T; Chen, F. Multiwfn: A Multifunctional Wavefunction Analyzer. *J. Comput. Chem.* **2012**, *33*, 580-592.

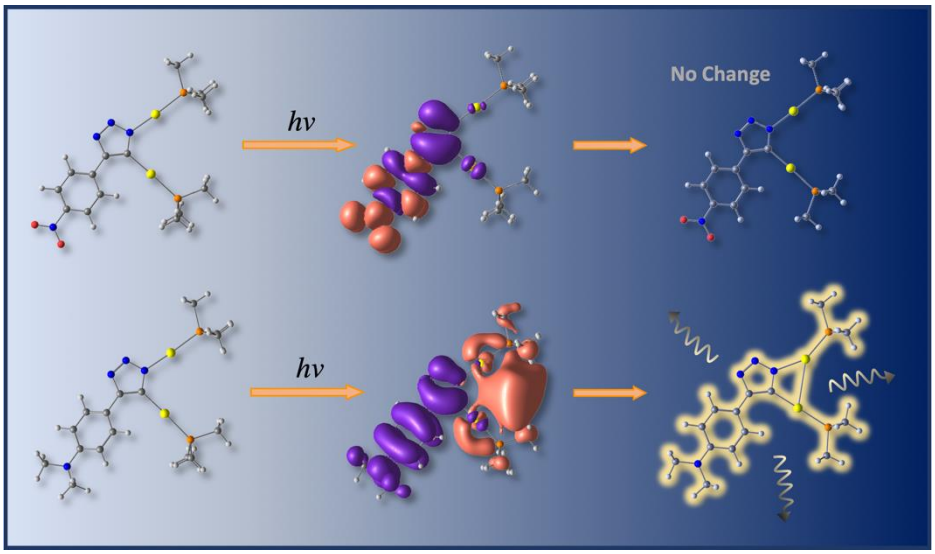

ToC Image